Study on Microstructures, Micro-hardness and Sensitization behavior in Heat Affected Zone (HAZ) of Type 316L Stainless Steel Joint With Narrow Gap Welds

S.I. Faisal

Bangladesh Atomic Energy Regulatory Authority, E-12/A, Agargaon, Dhaka-1207

Abstract

The welding zone is considered the most vulnerable part of the components. During the welding process Heat Affected Zone (HAZ) faces distinctive thermal experience comparing to the fusion line, for that these two zones have their unique microstructure properties and corrosion susceptibility. In nuclear power plants, the corrosion resistance of 316L stainless steel weld joints of several components and pipes may be affected by the formation of local sensitized zones. For safety and economy, a perfect and reliable structural integrity assessment of the main components in NPP is required as it is joined by different welding processes. In this study, 316L stainless steel welds were prepared by the automated Narrow Gap Welding (NGW) technique. The structural and corrosion relationships of base metal, HAZ, weld region with different welding thickness positions such as top, middle and bottom were investigated. Differences in microstructures features were observed in HAZ from weld and base metal, relating to grain size and ferrite contents. There was a little increase in micro-hardness values across the weld and HAZ. The Degree of Sensitization (DOS) was measured through the Double Loop Electrochemical Potentiokinetic Reactivation (DL-EPR) technique. The DOS values in weld regions were found larger than base metal and HAZ. The measured DOS in HAZ was less than 1%, which confirmed that HAZ was non-sensitized during NGW.

Keywords: Micro-hardness, Sensitization, Heat affected zone (HAZ), Degree of sensitization (DOS)

1. Introduction

Several components and pipes of nuclear power plants are joined by Narrow Gap Welding (NGW) process for less cost and time [1]. The cycle of heating and cooling that occurs during the welding process affects the microstructure and surface composition of welds and adjacent base metal. Microstructures formed in the weld and Heat Affected Zone (HAZ) determines the properties of the weld and their properties depend on heating, cooling rates (power, weld travel speed). Since heat transfer of metal is very fast, heated and partially melted base metal cooled down rapidly; then solid-state phase transformations occurred in the HAZ adjacent to the fusion line. A range of thermal cycles is experienced in the HAZ, depending on the distance from the fusion boundary. Because of the difference in maximum temperature and cooling rate of these two zones, have their own microstructural features and corrosion susceptibility in each position [2]. The welding zone, considered the weakest and failure initiation source of the components [3]. In nuclear power plants, 316L stainless steels are commonly used material for their metallurgical stability, high corrosion resistance, and good creep and ductility properties at elevated temperatures. Its corrosion resistance may be affected by the formation of local sensitized zones (i.e., regions susceptible to corrosion) that often develop on heating or cooling slowly in the temperature range 723K to 1123K [4]. During this high-temperature exposure, depletion of Cr to less than 12 wt. % occurs, which gives rise to precipitation of a continuous network of chromium-rich phase along critical zones, which is called sensitization. Sensitization of the HAZ is one of the major problems in the welding of austenitic stainless steel. Numerous failures have been attributed to the nuclear and petrochemical industries as a result of sensitization.

Corresponding author: *faisal83du@gmail.com*

For the safety and economy of nuclear power plants, an accurate and dependable structural reliability evaluation of the main components is needed as it is joined by different welding processes. The safe operation of nuclear power plants is reliant upon their structural integrity; consequently, the accurate design and lifetime assessment of welded joints are critical to improving the life-span of the whole plant. Various researches have been conducted primarily on the parent material and welded regions, but very limited studies have been conducted in the HAZ as well as in the weld thickness direction. Previously the fatigue crack growth rate and fracture toughness on HAZ of 316L stainless steel with NGW both in plant operating temperature and room temperature were evaluated [5]. But a few studies were carried out on microstructures and corrosion behavior on HAZ in different welding thickness layers.

In the present study, 316L stainless steel welds were prepared by automated NGW technique. The structural and corrosion relationships of the parent base metal, HAZ, and weld region along with three welding thickness positions such as Top, Middle, and Bottom were investigated. Microstructures analysis of this weld and HAZ in terms of grain morphology was evaluated. The volume fraction of phases (austenite and ferrite) was measured in these different regions by Optical Light Microscope (OLM). Micro-hardness was measured in HAZ, weld fusion zone, and base metal for three different positions by the Vickers microhardness process. Degree of Sensitization (DOS) of HAZ, weld zone, and base metal were measured through Double Loop Electrochemical Potentiokinetic Reactivation (DL-EPR) technique. It is a rapid and non-destructive way to evaluate the susceptibility to intergranular corrosion.

2. Materials and Method

2.1 Welding materials and sample preparation

Type 316L stainless steel was used for the base metal and 308L for the welding wire. The chemical compositions of both metals are shown in Table 1. Welding thickness was 76 mm. A detailed welding procedure was discussed in ref. [1]. The weld block was cut in the top, middle and bottom regions as shown in Fig. 1.

Table 1: Chemical composition of base metal and weldments (wt %)

Elements	C	Cr	Ni	Mo	Mn	Si	P	S	Nb+Ta	N	Fe
316L base metal	0.018	16.4	10.08	2.04	1.50	0.38	0.029	0.025	-	-	balance
308L weld wire	0.027	21.09	10.22	0.111	1.94	0.531	0.029	0.007	0.121	0.017	balance

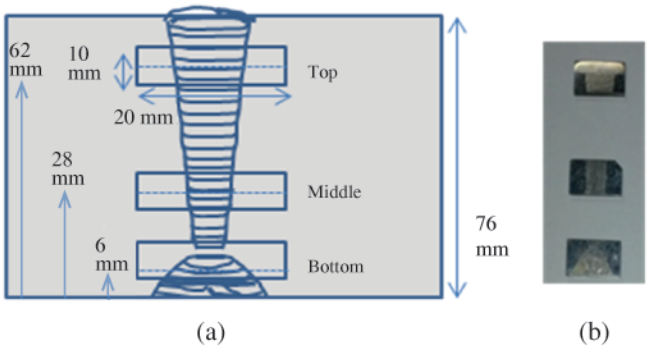

Fig. 1: (a) Sample collection positions (b) three collected samples in NGW for microstructure observation and micro hardness measurements

Weld and HAZ samples were collected by classifying their characteristic microstructures (base metal, HAZ, and weld metal) through an optical microscopic analysis and cut by IsoMet® 5000 precision saw & IsoMet™ low-speed precision cutter. The HAZ is the region between the fusion line and the base metal which is formed near the fusion zone as shown in Fig. 2.

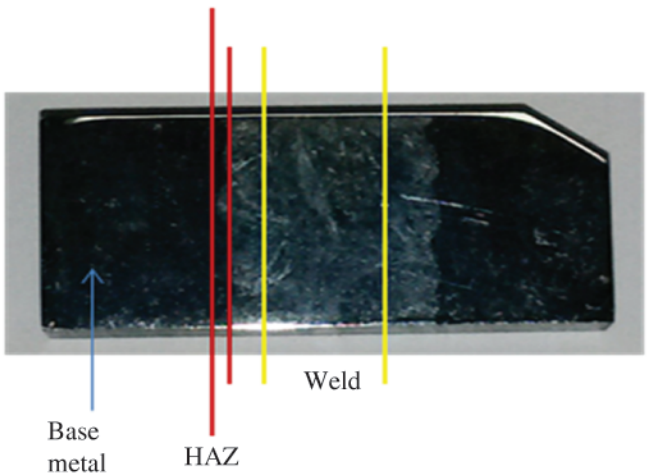

Fig. 2: Locations of HAZ and weld specimen

2.2 Microstructures observations and Phase volume fraction measurement

The sample was polished down to 1 µm with Silicon Carbide sandpaper and diamond paste using standard metallographic preparation technique and finally cleaned with pure ethanol and dried with air. The samples were etched with 1 HNO_3:1 HCl solution to reveal the microstructure of weld & HAZ by LOM. Optical microscopy was conducted using an OLYMPUS GX 51 microscope at various (5-100X) magnifications. Images were captured using analysis ts materials software.

OLYMPUS Image Analysis Software was used to identify the austenite & ferrite phases which present in the base metal, weld & HAZ. The mounted specimens were polished to a finish of one micron and electrochemically etched in 20 (wt. %) NaOH solution as described in ASTM A923 [6]. The electrolyte was selected to provide a distinction between the austenite and ferrite phases. The specimen to be etched was as an anode, and a piece of platinum metal as large as the specimen was made the cathode. The solution for etching was prepared by adding 20 g of reagent grade sodium hydroxide (NaOH) to 100 g of distilled water. The specimens were etched at 20V dc, for 5-10 s.

2.3 Vickers micro-hardness measurements

During the micro-hardness test, the sample surface was well polished without any fine scratches to minimize errors that might occur when indenting on these scratches. Vickers hardness measurements were made using a 100 g load for the base material, HAZ, and weld regions of the welded three sample positions. Hardness value was measured using 400 Series automated hardness tester with *Expert Hardness 2007 v2.0 software.*

2.4 Degree of sensitization (DOS) measurement

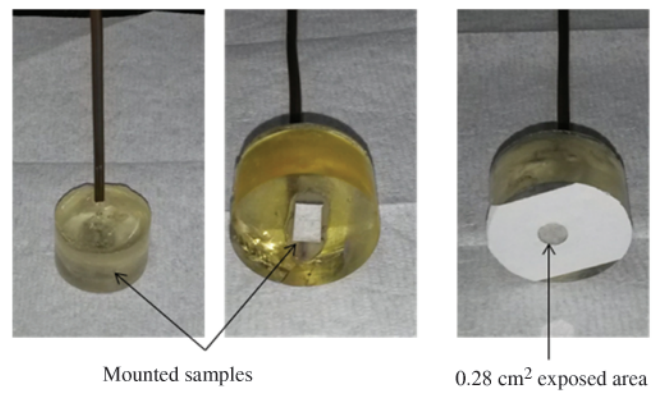

Fig. 3: Samples used for DL-EPR test

Specimen preparation and the polarization measurements for the DL-EPR test were performed according to ASTM G

108-94 (2010) [7]. The electrochemical testing samples were connected to a copper wire, mounted in epoxy cold resin to avoid the presence of crevices after the electric contact. Surfaces exposed to the electrolyte were prepared by sequential grinding with silicon carbide paper and polishing down to 1 micron with diamond paste. Fig. 3 shows the configuration of the samples used in the DL-EPR test. The exposed working area was 0.28 cm^2.

The DL-EPR tests were carried out using GAMRY potentiostat, a conventional electrochemical cell composed of a three-electrode setup. The sample under study is a working electrode equipped with a high purity graphite counter electrode and a saturated calomel reference electrode (SCE) in front of the sample. Fig. 4 shows the standard electrochemical cell and a photograph of the experimental setup with GAMRY potentiostat. All the tests were conducted in 0.5 M H_2SO_4 + 0.01 M KSCN electrolyte solution at room temperature (~ 30° C).

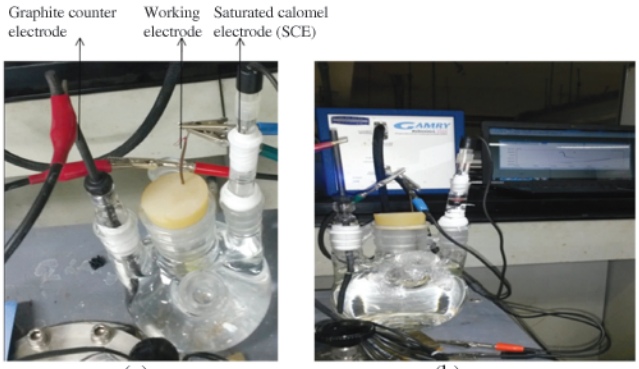

Fig. 4: (a) Electrochemical cell used in DL-EPR test (b) EPR test setting with GAMRY Instruments Reference 300

3. Results and Discussion

3.1 Microstructures characterization and Phase volume fraction

The developed microstructures are dependent on alloying elements, solidification behavior, and thermal cycles in welding processes. An optical micrograph of the base metal 316L stainless steel is shown in Fig. 5 of 500 µm scale.

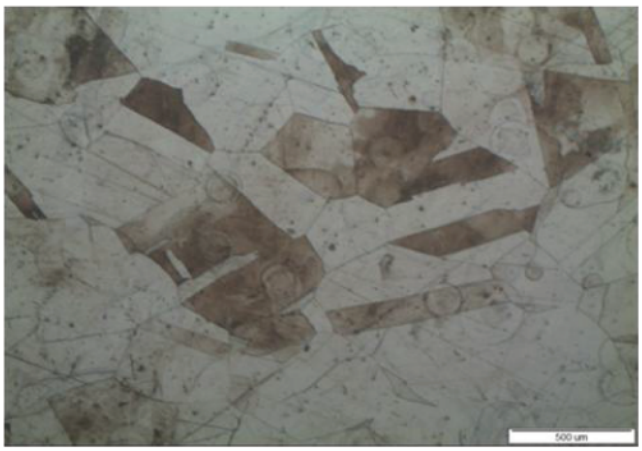

Fig. 5: Micrograph of base metal

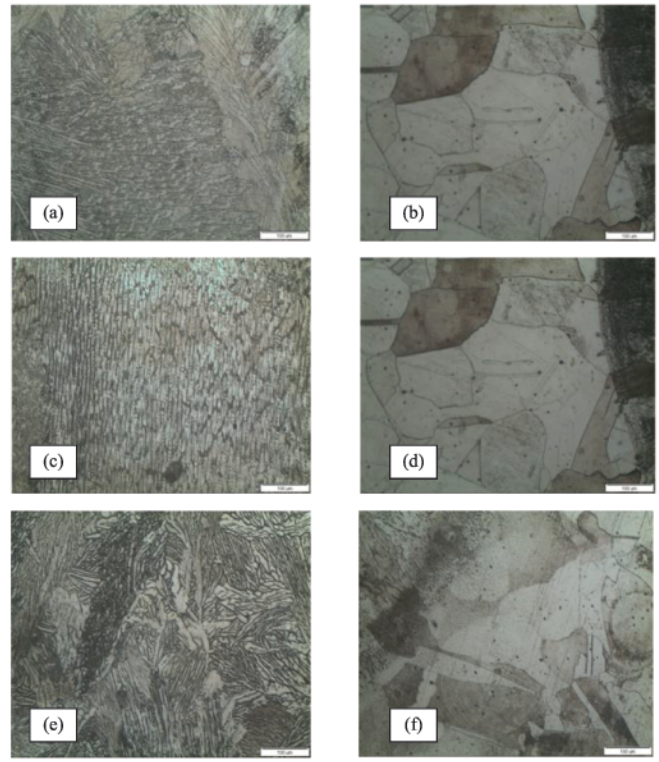

Fig 6: Micrograph of (a) Top weld (b) Top HAZ (c) Middle weld (d) Middle HAZ (e) Bottom weld (f) Bottom HAZ in 100 µm scale

In Fig. 6 (b,d,e) Microstructures in HAZ for Top, middle and bottom positions are similar to the base metal but the average grain size of the HAZ is a bit larger than the base metal. During welding, heated and partially melted base metal cooled down rapidly and phase transformation occurred in the HAZ [8, 9]. Near the fusion boundary on HAZ, shapes, and size of grains depend on locations [10]. Near the fusion boundary, the dendrite directions are perpendicular to the fusion line as shown in Fig.6 (a,c,e). Similar characteristics were reported in previous studies [5, 8].

Microanalysis reveals that the sample consists of ferrite and austenite phases. It colored the austenite in white, ferrite in light brown. The amounts of phases were estimated by measuring the fractions of the colored area on polished and etched specimens by light optical microscopy. The measured volume fractions of ferrite and austenite phases in different regions are given in Table 2.

Table 2: Phase volume fraction (%)

Position	Average Ferrite phase (%)	Average Austenite Phase (%)
Base_316L	1.56	98.44
Top_weld	19.51	80.48
Top_HAZ	2.34	97.65
Middle_weld	14.74	85.25
Middle_HAZ	4.3	95.69
Bottom_weld	15.24	84.76
Bottom_HAZ	5.46	94.54

From Table 2, the average measured ferrite volume fraction of base metal is 1.56 %. Ferrite content of three positions of the weld region is 19.51 %, 14.74 %, and 15.24 % for the top, middle, and bottom respectively. These measured values are nearly consistent with the ferrite number calculated from the Welding Research Council (WRC)-1992 diagram. According to Table 1, the used filler metal 308L contains a Chromium equivalent, Cr_{eq} = 21.09 and Nickel equivalent, Ni_{eq} = 10.22 and from these Cr_{eq} and Ni_{eq}, the WRC diagram indicates ferrite number, FN= 17. In Table- 2 ferrite phase volume fraction of the HAZ regions is varied between 2.34 % to 5.46 % for three thickness positions and the average is about 4.03 %, which is less than the weld zone, but higher than 316L base metal (1.56%). Since ferrite content above 3 vol. % usually guarantee primary ferrite formation and thus reduce hot cracking susceptibility. Again, ferrite above 10 vol. % can degrade mechanical properties at low and high-temperature service [11]. The measured ferrite content in HAZ is below 10% and ranging from an optimum condition (3% to 8%) for hot cracking resistance.

3.2 Vickers Micro-hardness

Micro-hardness measurement positions and results of the Vickers micro-hardness measurements of the top, middle, and bottom are graphically represented in Fig. 7(a)-(c). The hardness readings were taken at different regions indicating base metal-316L, weld-308L and HAZ for the two-sided welding approach. The distance was identified from the center of the weld and measured twice for each distance in a parallel line 200 µm apart. A little increase in hardness value on the HAZ of stainless steel NGW near fusion boundaries was observed in Fig. 7(a) - (c). This is because the phase structure of 316L base metal was not so much transformed by the temperature variations during welding [12]. This is in agreement with the literature reported [13] for industrial low carbon steel. The hardness values recorded in the HAZ were found to be around 239-273 $HV_{0.1;}$ 237-255 $HV_{0.1}$ and 227-255 $HV_{0.1}$ respectively for top, middle and bottom. By analyzing microstructure and observing micro-hardness variation in Fig.7, the HAZ area was identified approximately 1mm from the fusion line at both joined sides in the top, middle & bottom regions.

In the welded 308L variation of hardness values were ranging around 225-247 $HV_{0.1;}$ 220-255 $HV_{0.1}$ and 220-258 $HV_{0.1}$ respectively for top, middle, and bottom. Hardness values were a little increase at the bottom of the weld and decrease in the middle and top of the weld. Similar behavior was reported [10] in the Inconel weld. Hardness values ranging from 210 $HV_{0.1}$ to 250 $HV_{0.1}$ were observed for 316L of the base metal. Slightly higher hardness values were observed in the weld 308L region compares to the base 316L. This might be correlated to moderate values of ferrite content, average grain size and a higher concentration of interstitial atoms (such as C and N) compare with base metal with no N and less C (0.018 wt% in 316L base & 0.027 wt% in weld 308L).

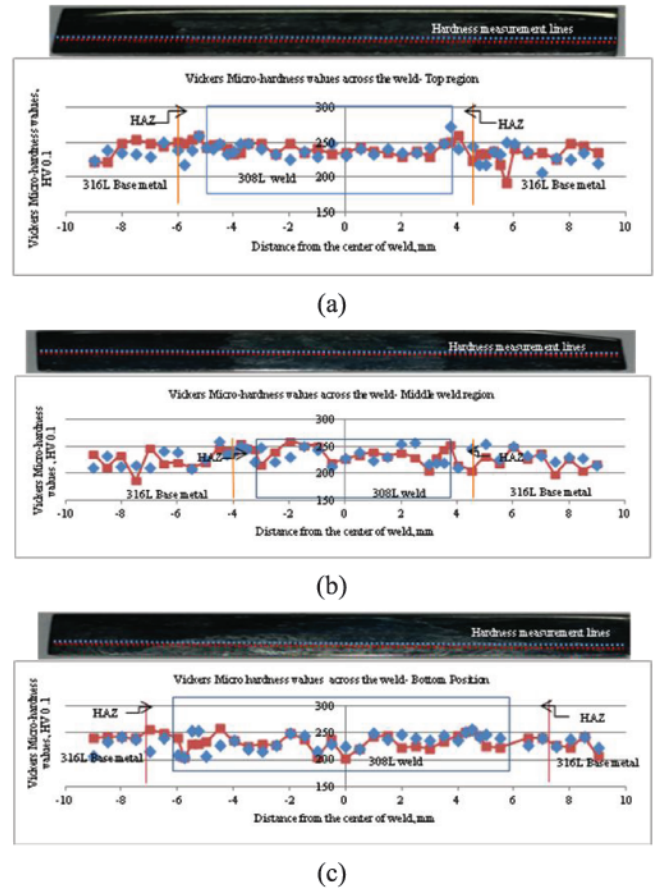

Fig. 7: Vickers Micro-hardness results in the (a) Top position (b) Middle position (c) Bottom position

3.3 Degree of Sensitization (DOS)

Cyclic polarization curves of the DL-EPR method for base metal, HAZ and weld regions are respectively represented in Fig. 8 (a-c). DOS measurements from Fig. 8 (a-c) are shown in Table 3(a-c). The test was repeated twice for each region to ensure reproducibility. DL-EPR Cyclic polarization curves were obtained in two steps: Firstly, the working electrode was subjected to open-circuit conditions, until a steady-state potential (E_{corr}) was reached. It takes 3 minutes to reach a steady-state value. Secondly, an anodic potentiodynamic sweeping rate of 1.67 mV/s (6 V/hr) from the back of open circuit potential (~ -500 mV/E_{corr}) to +300 mV_{SCE} was imposed. When the potential is increased above the specimen open circuit potential (E_{corr}), the specimen behaves anodically. As a result, the rate of corrosion (metal dissolution reaction) rises rapidly in the activation range up to a point when the activation peak current density (I_a) is reached. This is because; the activation or critical current density (I_a) or (I_{crit}) is proportional to the corrosion rate of the metal. Again, when the potential is raised further, the anodic current dropped to a lower value called passivation current density (I_{pass}), and then it remains constant over a wide potential range. This is the passive range, in which a thin, invisible film of oxide covers the metal surface. This protective film acts as a barrier between the metal and its environment and reduces the rate of dissolution. Then at the same scan rate from +300 mV_{SCE}, the potential scanning

was reversed back cathodically polarized to -500 mV/ E_{corr}. This range of polarization scans was chosen to ensure that sample was brought into the passive domain.

During the anodic sweep, the entire surface is active and contributes to the peak current, while during the reactivation sweep only the sensitized regions contribute to the passive-active transition. The current on the reverse scan is assumed to be primarily due to the reactivation of the chromium depleted grain boundaries. As a result, the ratio (I_r/I_a) of the reactivation current peak (I_r) to the activation current peak (I_a) is used to establish the degree of sensitization where a value less than 1% indicates material is not sensitized and a value equal to or higher than 1% indicates that the material is sensitized [14]. For DOS measurement, the peak current of the anodic nose from the first anodic polarization (I_a) is compared to the peak current on the reactivation scan (I_r) [15]. The average DOS for base metal- 316L stainless steel in Table 3(a) was measured as 0.56%; which is less than the criteria for the sensitized zone (DOS >1%). Hence it indicates the absence of sensitization phenomena within the base metal.

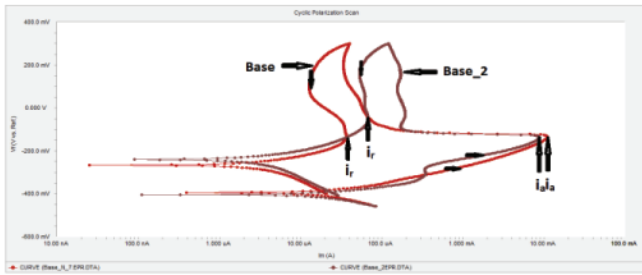

a)

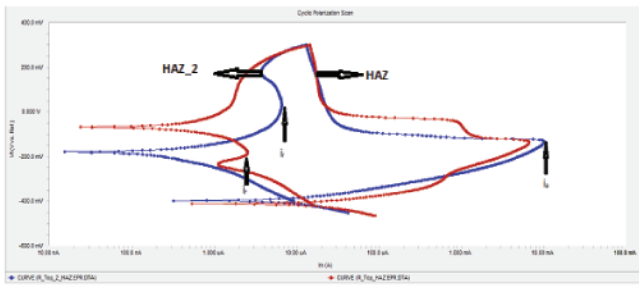

b)

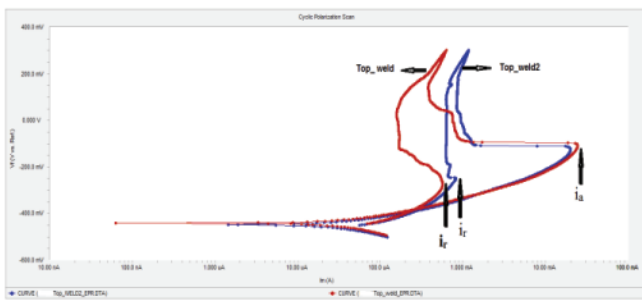

c)

Fig 8: DL_EPR curves of a) base metal-316L b) Top_HAZ c) Top_weld

Table 3(a): DL-EPR test results obtained from polarization curves of base metal-316L

Sample	i_r (A)	i_a(A)	DOS [i_r/i_a] *100 (%)	Average DOS (%)
Base	36.5×10^{-6}	10.96×10^{-3}	0.33	0.56
Base_2	66.98×10^{-6}	8.53×10^{-3}	0.78	-

Table 3(b): DL-EPR test results obtained from polarization curves of Top_HAZ

Sample	i_r (A)	i_a(A)	DOS [i_r/i_a] *100 (%)	Average DOS (%)
Top_HAZ	2.532×10^{-6}	6.635×10^{-3}	0.038	0.051
Top_HAZ_2	6.513×10^{-6}	10.05×10^{-3}	0.064	-

Table 3(c): DL-EPR test results obtained from polarization curves of Top _weld

Sample	i_r (A)	i_a(A)	DOS [i_r/i_a] *100 (%)	Average DOS (%)
Top_weld	568.7×10^{-6}	24.19×10^{-3}	2.35	3.24
Top_weld_2	819.1×10^{-6}	19.83×10^{-3}	4.13	-

Fig. 8(b) and Fig. 8(c) show the polarization curves of the DL-EPR test for the Top_HAZ and Top_weld region respectively. Measured average DOS in weld 308L was found 3.24% and HAZ was 0.051% as shown in Table 3(b) and Table 3(c). From Tables 3(a)-(c), the weld region contains higher DOS than base metal and HAZ. A higher C content in weld 308L compare to base 316L may contribute to higher DOS in the weld to base metal by forming more Cr-carbide precipitation. Besides, in the weld zone, there is a formation of the δ-ferrite phase which was confirmed by phase volume fraction measurement through OLM, and the measured δ-ferrite was higher than optimal values (3% to 8% for preventing to form of continuous carbide network) [11]. This high δ-ferrite could contribute to forming a continuous network of carbides and which increased the DOS in the weld. Also, because of the lower carbon solubility in the δ-ferrite phase [16] which results in the matrix supersaturation and the consequent precipitation of the Cr-carbides those were adjacent to the δ-ferrite phase.

However, when comparing the average DOS on HAZ samples (0.051%) to the base metal (0.56%) and weld (3.24%) samples from Table 3, a much lower DOS is obtained because of the Cr-carbide precipitates possibly re-dissolution at the HAZ. That process occurred due to the thermal heat gradients in high-temperature on the HAZ, which is proper to the precipitates re-dissolution [17]. Furthermore, reduced time for the Cr-carbide precipitation could also contribute to the DOS lower levels in that region due to the high cooling rate [18] during the welding process. This enabled a very short remaining time in the Cr-carbide precipitation region and a lower alloying element microsegregation which led to reduced intergranular corrosion susceptibility.

Fig. 9 shows the combined DL-EPR curve of three regions (base, HAZ, and weld) in the middle position and Table 4

presents the measured DOS. These indicate that the peak activation current densities (I_a) of the HAZ region were the same order of magnitude as compared with the base metal but I_a values of the weld region are almost three times higher than the base and HAZ region. Hence, the corrosion rate of the weld region is much higher compared to the base metal and HAZ region. The development of a reactivation peak during reverse scanning indicates that the oxide has dissolved and can be attributed to a metal dissolution reaction occurring within the sensitized regions. Consequently, lower reactivation peaks indicate incomplete dissolution of the passive oxide film while higher reactivation peaks indicate the complete dissolution of that protective oxide film. Since the peak reactivation current densities (I_r) in the weld region were big different from base metal and HAZ region which contributes higher DOS in the weld.

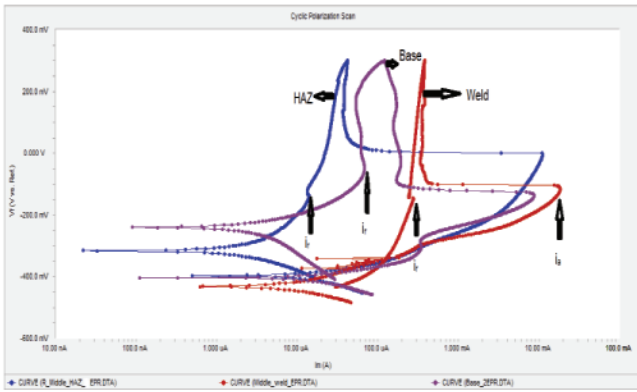

Fig. 9: Combined (base, HAZ,and weld) DL-EPR curves in three regions for middle position

Table 4: DL-EPR test results of middle position obtained from polarization curves

Sample	i_r (A)	i_a(A)	DOS [i_r/i_a]* 100 (%)
Base	66.98 x10^{-6}	8.53 x10^{-6}	0.785
Middle_HAZ	13.92 x10^{-6}	10.88 x10^{-6}	0.127
Middle_Weld	276 x10^{-6}	18.15 x10^{-6}	1.52

DL-EPR curves (Fig. 9) and Table 4 present very similar activation current densities for the base and HAZ, However, the base metal has relatively more DOS (0.785 %) than the HAZ (0.127 %), this is because of more reactivation current densities (66.98 µA for base metal) than HAZ (13.92 µA).

The comparative results of DOS values, as well as the activation and reactivation current densities, are obtained from the polarization curve for three regions (base, HAZ, and weld) presented in Fig. 10. The lowest Degree of Sensitization (DOS), relatively low activation current density (I_a), and lowest reactivation current density (I_r) was observed for the HAZ while the highest degree of sensitization, highest activation current density (I_a), and highest reactivation current density (I_r) was observed for the weld 308L region.

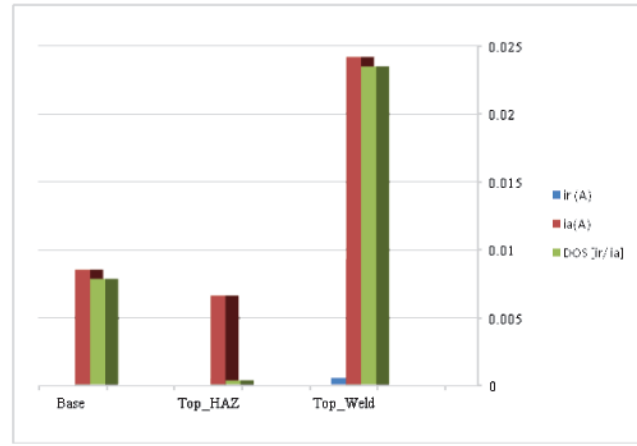

(a)

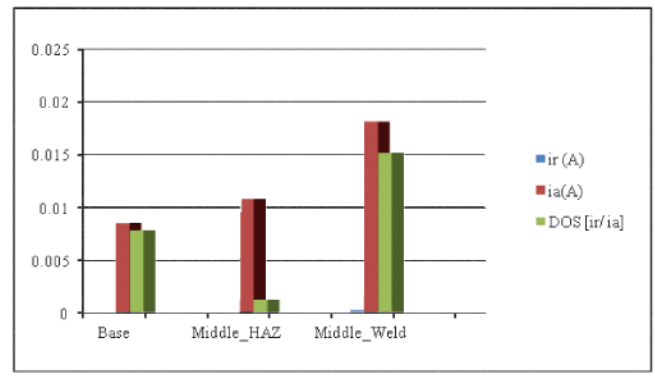

(b)

Fig. 10: Comparative results of the DL-EPR test in (a) Top Position (b) Middle Position

4. Conclusion

This study brings up an insight to understand the NGW effects in HAZ for the microstructural and sensitization behavior of 316L stainless steel that has a critical influence on the integrity of nuclear components welds. Microstructures variation related to grain size was observed between the HAZ and weld region in different weld thickness positions. This may be associated with different thermal cycles and subsequent different cooling rates in the HAZ and weld region during the welding process. The average value in HAZ was nearly 4.03% ferrite. Since the 10% ferrite is the maximum value to prevent degradation of mechanical properties at low- or high-temperature service, so the HAZ can sustain mechanical degradation in such conditions. A gradual increase in hardness values across the joints was observed. The reason for this little hardness change in the HAZ region is considered that the phase structure of base 316L was not so much transformed by the temperature variations during NGW. DL-EPR test confirmed that 316L NGW HAZ was not susceptible to sensitization as DOS <1%. The main reason for low DOS in HAZ was estimated due to the lower carbon content and the insufficient precipitation time for these specimens. This work can provide a foundation for future work involving dissimilar metal welds used in nuclear components. It will also be the basis to evaluate the weld materials properties at

plant operating temperatures in the nuclear power plant and other works.

Acknowledgment

The author would like to acknowledge the Korea Advanced Institute of Science and Technology lab for providing the facilities during the experiments and the Korea Institute of Nuclear Safety in support of sponsorship.

References

1. C. Jang, P.Y. Cho, M. Kim, S.J. Oh and J.S. Yang, Effects of Microstructure and Residual Stress on Fatigue Crack Growth of Stainless Steel Narrow Gap Welds, Materials and Design, **31**(4)**,** 1862-1870 (2010).
2. J.R. Davis & Associates, Corrosion of Weldments, (USA: ASME International) 1-10 (2006).
3. M.E.W. Steve, H. Jeffrey, Welding for New Nuclear Power Plants, Welding Journal, **88,** 40-43 (2009).
4. H. Shaikh, B.P.C. Rao, S. Gupta, R.P. George, S. Venugopal, B. Sasi, T. Jayakumar and H.S. Khatak; Assessment of Intergranular corrosion in AISI Type 316L Stainless steel weldments, British Corrosion Journal, **37**(2),129-140 (2002).
5. H.J. Lee, M. Kim, C. Jang, S.Y. Cho and J.S. Yang, Fatigue Crack Growth Rate and Fracture Resistance of Heat Affected Zone of Type 316L Stainless Steel with Narrow Gap Welds, ASME Pressure Vessels & Piping Division Conference, (17-21 July 2011)
6. ASTM A923, Standard Test Methods for Detecting Detrimental Intermetallic Phase in Duplex Austenitic/Ferritic Stainless Steels, (USA: ASTM International).
7. ASTM G108-94, Standard Test Method for Electrochemical Reactivation (EPR) for Detecting Sensitization of AISI Type 304 and 304L Stainless Steels, (USA: ASTM International) (2010).
8. C. Jang, J. Lee, J.S. Kim and T.E. Jin, Mechanical property variation within Inconel 82/182 Dissimilar Metal Weld Between Low Alloy Steel and 316 Stainless Steel, Int. Journal of PVP, **85**, 635–646 (2000).
9. P. Zahumensky, S. Tuleja, J. Orszagova, J. Janovec and V. Siladiova, Corrosion resistance of 18Cr-12Ni-2.5Mo steel annealed at 500-1050°C, Corrosion Science, **41**(7), 1305-22 (1999).
10. D.A. Porter and K.E. Easterling, Phase transformations in materials and alloys, (England: Van Nostrand Reinhold Co.), 373-376 (1981).
11. D.L. Olson, T.A. Siewert, S. Liu and G.R. Edwards, Editors, ASM Handbook, Welding, Brazing and Soldering, Book Chapter: A. Wahid, D.L. Olson and D.K. Matlock, Corrosion of Weldments, **6** 1065-1069 (1993).
12. A.Celik and A. Asaran, Mechanical and structural properties of similar and dissimilar steel joints, Materials Characterization, **43,** 311–318 (1999).
13. B.Zakaria, D. Chemseddine and T. Baudin, Effect of Welding on Microstructural and Mechanical Properties of an Industrial Low Carbon Steel, Scientific Research Engineering, **2,** 502-506 (2010).
14. A. Turnbull, P.E. Francis, M.P. Ryan, L.P. Orkney, A.J. Griffiths and B. Hawkins, A Novel Approach to Characterizing the Corrosion Resistance of Super Duplex Stainless Steel Welds, NACE International, **58(12),** 1039-1048 (2002).
15. A.P. Majidi and M.A. Streicher, Potentiodynamic Reactivation Method for Detecting Sensitization in AISI 304 and 304L Stainless Steels, Corrosion, **40**(8), 393–408 (1983).
16. E. Folkhard, Welding Metallurgy of Stainless Steel, 1st ed., (USA: Springer-Verlag) (1988).
17. O.M. Akselsen, G. Rorvik, P.E. Kvaale and C. van der Eijk, Microstructure-property Relationships in HAZ of new 13% Cr Martensitic Stainless Steels, Welding Journal, **83,** 160-167 (2004).
18. S.A. David, S.S. Babu and J.M. Vitek, Welding: Solidification and Microstructure, Journal of Minerals, Metals, and Materials Society, **55,** 14-20 (2003).